RESEARCH ARTICLE

Key Points:
- Eddy-driven transport cannot explain preferred sedimentation over Zapiola Rise
- The Zapiola Anticyclone is a barrier for mixing
- Resuspension may be critical to the existence of the Zapiola Rise

Correspondence to:
W. Weijer,
wilbert@lanl.gov

Eddy-driven sediment transport in the Argentine Basin: Is the height of the Zapiola Rise hydrodynamically controlled?

Wilbert Weijer[1], Mathew E. Maltrud[2], William B. Homoky[3], Kurt L. Polzin[4], and Leo R. M. Maas[5]

[1]Computational, and Statistical Sciences Division, Los Alamos National Laboratory, Los Alamos, New Mexico, USA, [2]Theoretical Division, Los Alamos National Laboratory, Los Alamos, New Mexico, USA, [3]Department of Earth Sciences, University of Oxford, Oxford, UK, [4]Department of Physical Oceanography, Woods Hole Oceanographic Institution, Woods Hole, Massachusetts, USA, [5]Department of Physical Oceanography, Royal Netherlands Institute for Sea Research, den Burg, Netherlands

Abstract In this study, we address the question whether eddy-driven transports in the Argentine Basin can be held responsible for enhanced sediment accumulation over the Zapiola Rise, hence accounting for the existence and growth of this sediment drift. To address this question, we perform a 6 year simulation with a strongly eddying ocean model. We release two passive tracers, with settling velocities that are consistent with silt and clay size particles. Our experiments show contrasting behavior between the silt fraction and the lighter clay. Due to its larger settling velocity, the silt fraction reaches a quasisteady state within a few years, with abyssal sedimentation rates that match net input. In contrast, clay settles only slowly, and its distribution is heavily stratified, being transported mainly along isopycnals. Yet, both size classes display a significant and persistent concentration minimum over the Zapiola Rise. We show that the Zapiola Anticyclone, a strong eddy-driven vortex that circulates around the Zapiola Rise, is a barrier to sediment transport, and hence prevents significant accumulation of sediments on the Rise. We conclude that sediment transport by the turbulent circulation in the Argentine Basin alone cannot account for the preferred sediment accumulation over the Rise. We speculate that resuspension is a critical process in the formation and maintenance of the Zapiola Rise.

1. Introduction

The Argentine Basin (AB) in the southwestern South Atlantic is a fascinating region, both from an oceanographic and a geological perspective. The basin of approximate circular shape is bounded by the Falkland escarpment to the south, the South American continent to the west (Patagonian Shelf), the Rio Grande Rise to the north, and the Mid-Atlantic Ridge to the east (Figure 1). Ocean depths exceed 6000 m in the southwestern part of the basin. A curious feature, and the subject of this study, is the Zapiola Rise (ZR), a sediment drift in the center of the basin that rises to 4700 m below the surface [*Ewing et al.*, 1964; *Le Pichon et al.*, 1971]. Extensive seismic surveys have established that the ZR is the summit of a sedimentary complex that reaches a thickness of no less than 3 km [*Ewing et al.*, 1964; *Whittaker et al.*, 2013]. The sediments appear to have been deposited in smooth layers on rugged bedrock; nonetheless, the surface of the deposit is covered with mudwaves with heights of up to 150 m and wave lengths of up to 10 km [*Ewing et al.*, 1971; *Klaus and Ledbetter*, 1988; *Flood and Shor*, 1988; *Flood et al.*, 1993].

The oceanography of the region is complex (Figure 2) [*Reid*, 1989; *Peterson and Stramma*, 1991; *Peterson*, 1992]. At shallow levels, it is dominated by the energetic Malvinas and Brazil Currents and their confluence (Brazil/Malvinas Confluence; BMC). The Brazil Current is the western boundary current of the South Atlantic subtropical gyre, and feeds into the South Atlantic Current that flows along the Subtropical Front. The Malvinas Current is a branch of the Antarctic Circumpolar Current (ACC) that sweeps north after passing through the Drake Passage. The BMC at 38°S is highly variable due to baroclinic instabilities and wind variability [*Garzoli and Simionato*, 1990; *Garzoli*, 1993; *Garzoli and Giulivi*, 1994]. It gives rise to intense eddy formation and exceptionally high levels of eddy kinetic energy (Figure 2, shading) [*Fu and Smith*, 1996]. Eddy variability is highest in the BMC zone and displays a distinctive minimum over ZR. This eddy activity is responsible for significant modifications of the water masses passing through the basin, like Antarctic Intermediate Water, Subantarctic Mode Water, and Circumpolar and North Atlantic Deep Water [*Jullion et al.*, 2010].
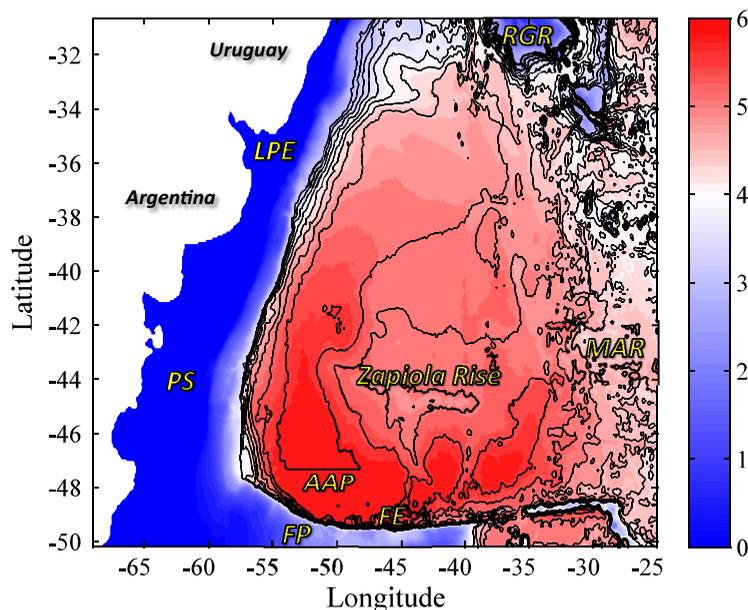
Figure 1. Bathymetry of the Argentine Basin (shading; km); and distribution of barotropic potential vorticity f/H (where f is the Coriolis parameter and H is water depth), as represented in the POP model. Contours show $\log_{10}|f/H|$, from -8.0 to -7.6, stride 0.025, where the argument is understood to be nondimensionalized by $1 m^{-1} s^{-1}$. Features indicated are Zapiola Rise; La Plata Estuary (LPE); Patagonian Shelf (PS); Falkland Escarpment (FE) and Plateau (FP); Mid-Atlantic Ridge (MAR); Rio Grande Rise (RGR); and Argentine Abyssal Plain (AAP). Note that maximum depth in the AAP (6212 m) exceeds depth range of the model.

A unique feature of the circulation in the Argentine Basin is the Zapiola Anticyclone (ZA). The ZA is an anticyclonic gyre that circulates around the crest of the ZR in a nearly barotropic fashion. The presence of a strong anticyclonic circulation was deduced first by *Flood and Shor* [1988], based on photographic evidence for bottom flow direction, and the orientation of the mud waves. Current meter records were consistent with these observations [*Weatherly*, 1993]. The first full-depth observation of the ZA was presented in *Saunders and King* [1995], who analyzed hydrographic and ADCP (Acoustic Doppler Current Profiler) observations from a trans-Atlantic cruise. In more recent years, the presence of the ZA has been confirmed by drifter observations [*Boebel et al.*, 1999]; feature tracking studies using altimeter data [*Fu*, 2006]; and estimates of the ocean's mean dynamic topography (MDT), through a combination of remote sensing and in situ observations [e.g., *Maximenko et al.*, 2009].

Reliable estimates of the transport of the ZA remain scarce, however. *Saunders and King* [1995] suggested that the ZA represents a volume transport of no less than 100 Sv (1 Sv = $10^6 m^3 s^{-1}$). Even so, this value may be an underestimation. Their Figure 15 shows a

Figure 2. Vertically integrated eddy kinetic energy per unit area (shading; $10^6 kg s^{-2}$); and distribution of barotropic stream function (contours; interval 25 Sv, zero-contour in red), as represented by the POP model. Arrows schematically indicate the major flow features, in particular the Zapiola Anticyclone; the Malvinas Current (MC), Brazil Current (BC), and their confluence (BMC); the South Atlantic Current (SAC) and the associated Subtropical Front (STF); and the continuation of the Antarctic Circumpolar Current (ACC) along the Subantarctic Front (SAF).

maximum transport of 175 Sv close to 42°W, and zero crossings on either side at 49°W and 34°W. If the ZA were to account for only 100 Sv of this 175 Sv recirculation, a net transport of 75 Sv would need to be drawn southward between the ZR and the continent from the subtropical domain; this in addition to a complete recirculation of the Malvinas Current. Since 75 Sv is more than even the Brazil Current can deliver [*Peterson*, 1992], and most of its transport is thought to continue as the South Atlantic Current *north* of the ZR [*Peterson and Stramma*, 1991], a ZA transport close to 175 Sv may be a more appropriate interpretation of their data. *Saraceno et al.* [2009] report a mean strength of 50 and 40 Sv, based on two estimates of MDT. Numerical models show a wide range of transports, since the ZA is very dependent on the representation of bathymetry, and on frictional parameterizations and parameters [*De Miranda et al.*, 1999; *Penduff et al.*, 2001; *Barnier et al.*, 2006; *Penduff et al.*, 2007; *Combes and Matano*, 2014]. This holds true for data-constrained ocean models as well: *Volkov and Fu* [2008] find a mean transport of 100 Sv in the ECCO2 ocean state estimate, while the estimates of *Penduff et al.* [2002] and *Mazloff et al.* [2010] do not feature a ZA at all. Interestingly, *Volkov and Fu* [2008] and *Saraceno et al.* [2009] find strong variability in the transport estimates, that may be the low-frequency response to noisy eddy forcing [*Venaille et al.*, 2011]; and even episodes of cessation that they interpret as collapses of the anticyclone [*Bigorre and Dewar*, 2009].

The dynamics of this anticyclone was explained by *Dewar* [1998]. He shows that the crest of ZR is high enough to lead to a local extremum in barotropic potential vorticity f/H (where f is the Coriolis parameter, and H is total water depth; Figure 1). The tendency of the ubiquitous eddy field to homogenize vorticity leads to a mass convergence over the seamount, raising ocean pressure, and giving rise to an anticyclonic circulation. The bottom friction experienced by this circulation generates a divergent bottom Ekman transport, which closes the secondary circulation. Numerical analyses confirm that the ZA is consistent with this theory [*De Miranda et al.*, 1999; *Bigorre*, 2005; *Volkov and Fu*, 2008; *Bigorre and Dewar*, 2009].

The provenance of the sedimentary materials in the Argentine Basin is rather diverse. Surprisingly, a detailed analysis of the composition of the sediments that make up ZR is hard to find in published literature, but several studies can provide some insight in the composition of ZR sediments. Biogenic components in abyssal AB sediments appear to be dominated by Antarctic diatoms [*Jones and Johnson*, 1984; *Romero and Hensen*, 2002; *Manley and Flood*, 1993] and radiolarians [*Ewing and Lonardi*, 1971; *Zimmerman et al.*, 1979]. Since the crest of the ZR is below the Carbonate Compensation Depth (CCD), calcareous remains are mostly absent. The lithogenic component is dominated by clays and silts [*Biscaye*, 1965; *Balsam and Wolhart*, 1993; *Manley and Flood*, 1993]. This terrigenous material is most likely derived from the Patagonian Shelf [*Lonardi and Ewing*, 1971]. With an estimated sediment discharge of 92Mtyr^{-1}, *Milliman and Meade* [1983] list La Plata as the 14th largest river globally in terms of sediment discharge, 4th largest of South America, and by far the dominant contributor to the 154Mtyr^{-1} discharge into the South Atlantic Ocean. Other studies dispute La Plata as the main source for sediments, and point to more southerly segments of the Patagonian Shelf: *Pierce and Siegel* [1979] suggest a dominant contribution from erosion of coastal cliffs; while *Biscaye* [1965] and *Krinsley et al.* [1973] even suggest Antarctic origins of the sediments, carried into the AB by the strong Antarctic Bottom Water transport [*Le Pichon et al.*, 1971]. *Gaiero et al.* [2003] conclude that there is a significant aeolian input as well. Indeed, estimates of dust deposition compiled by *Mahowald et al.* [2005] range between 5 and 35 Mtyr^{-1} for the South Atlantic, with a significant fraction entering the Argentine Basin under the Patagonian dust plume.

How the coastal sediments reach the abyss is not quite clear. *Matano et al.* [2014] show how the freshwater plume from the Rio de la Plata is drawn into the interior of the AB by the BMC on a seasonal [and interannual, according to *Piola et al.*, 2005] basis, and it is probable that a significant part of its suspended sediment load undergoes the same fate. For sources along the southern Patagonian shelf, *Pierce and Siegel* [1979] conclude there is very little cross-shelf transport, although *Matano et al.* [2010] argue for at least some cross-shelf exchange between shelf waters and the MC. In any case, it is likely that sediments undergo repeated resuspension before finally making it across the shelf break. An important contributor to this process may be the strong tidal currents [*Allen et al.*, 1980] in La Plata estuary and on the Patagonian Shelf, which are among the strongest in the world [*Glorioso and Flather*, 1995, 1997; *Palma et al.*, 2004]. Alternatively, it is possible that a significant amount of sediment reaches the deeper AB through turbidite currents via an intricate network of submarine canyons that transects the continental slope [*Lonardi and Ewing*, 1971].

The topographic control exerted by the ZR on the ZA, and the apparent hydrodynamic control of the sedimentation processes that must have generated the ZR suggest a strong coupling between bathymetry, circulation, and sediment transport. What is more, analysis of the mud wave fields suggest that flow conditions around ZR must have been stable for at least 100 kyr [*Flood and Shor*, 1988; *von Lom-Keil et al.*, 2002]. However, explaining the existence of the sediment body in the center of the AB is not straightforward. If the sediment buildup on top of the ZR were to result mainly of bed-load transport, then this would require the transport to not only be upslope towards the crest of the ZR, but also upstream against the divergent bottom Ekman transport (implied by the secondary circulation of the ZA). Hence it seems more likely that the ZR results from processes involving *suspended* sediment transport. Indeed, the AB houses an intense nepheloid layer of suspended particulate matter [*Ewing et al.*, 1971; *Biscaye and Eittreim*, 1977; *Richardson et al.*, 1993; *Saunders and King*, 1995], generally ascribed to the presence of strong eddy activity and the generation of benthic storms [*Richardson et al.*, 1993]. It was suggested early on [*Ewing*, 1965; *Ewing et al.*, 1971; *Flood and Shor*, 1988] that the sediment is carried along by AABW when it fills the deep layers of the AB. With the AABW circulation concentrated along the South American continental margin in an energetic deep western boundary current, this would allow preferred sedimentation offshore where bottom velocities are weaker (Figure 2). This idea is supported by the grain size analysis of *Ledbetter* [1986], who found a minimum in mean size of silt particles over the ZR.

Still, for the ZR to be a site of preferred sedimentation, the ocean circulation would need to sustain a strong sediment transport towards the ZR; this in the face of a secondary circulation that most likely favors *divergent* sediment transport, and of a vortex that possibly hinders exchanges through its boundary. Here we address the hypothesis that the ocean circulation, and in particular the spatially varying field of eddy activity, acts to converge sediments over Zapiola Rise. We use a global ocean model of eddy resolving (nominally 0.1°) resolution to study the dispersion of sediment in two size classes through the Argentine Basin. These sediments are modeled as passive tracers ("dye") with settling velocities that are characteristic for silt and clay size particles. The source of these sediments in our model is La Plata estuary.

The structure of the paper is as follows: first we introduce the modeling approach, then describe the main results of the investigation; in particular an evaluation of the dynamics of the ZA, a description of the sediment distributions, and an analysis of the sediment budgets. This is followed by a discussion and conclusion.

2. Methods

To study the sediment dispersion in the Argentine Basin we perform a numerical experiment with Los Alamos National Laboratory's Parallel Ocean Program (POP) [*Dukowicz and Smith*, 1994]. The model is global in extent, and has a nominal grid spacing of 0.1°, which allows the explicit representation of energetic mesoscale features including eddies and boundary currents [*Maltrud et al.*, 2008, 2010]. The 42 levels range from a thickness of 10 m at the surface to 250 m at depth, and cover a maximum depth of 6000 m. An accurate and smooth representation of topographic slopes is achieved by the use of partial bottom cells [*Adcroft et al.*, 1997]. A quadratic bottom stress is applied to the momentum equations, with drag coefficient $C_d = 1 \cdot 10^{-3}$. This generic value is on the low end of observational estimates [e.g., *Weatherly*, 1984]. A low value of C_d seems justified given the smoothness of the bed forms in the Argentine Basin, but a higher value would probably have reduced the strong bias of the ZA in this model, as discussed later.

The simulation of 6 years was started from a 150 year long integration described in *Weijer et al.* [2012]. The atmospheric state was derived from the repeat annual cycle (normal-year) Coordinated Ocean Reference Experiment (CORE) forcing data set [*Large and Yeager*, 2004], with the 6 hourly forcing averaged to monthly means. So the seasonal cycle is the only externally enforced time scale in the system; all other time scales of variability are internally generated. Wind stress was calculated offline using the Hurrell Sea Surface Temperature (SST) climatology [*Hurrell et al.*, 2008] and standard bulk formulae [*Large and Pond*, 1982]. Sensible heat flux and evaporation were calculated online also using bulk formulae and the model predicted SST. Precipitation was also taken from the CORE forcing data set. Monthly river runoff from 46 major rivers [*Fekete et al.*, 1999] was added to the freshwater flux at the locations of the actual outflow, with the remaining ungauged runoff distributed evenly along the coasts of all of the continents. As explained in *Weijer et al.* [2012], in year 76 a salinity restoring term was replaced by its implied flux to run under mixed boundary

Barotropic streamfunction (f/H contours)
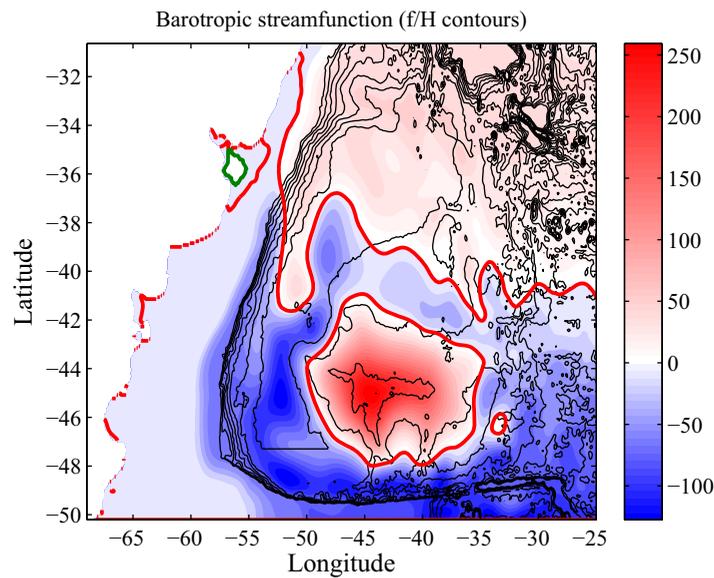
Figure 3. Mean barotropic stream function in Sv (shading). Black contours represent potential vorticity f/H; red contour represents $\Psi=0$, and the contour surrounding ZR is considered to be the boundary of the Zapiola Anticyclone. Green contour indicates sediment source area.

conditions. Monthly averaged fields of select variables were saved, as well as instantaneous snapshots every 5 days of the horizontal velocity and sediment fields at the depths of 15, 1875, and 3875 m, as well as vertically integrated quantities.

Sediment is modeled as concentrations C (in gm^{-3}) of passive dye, advected by the three-dimensional circulation, but with an additional vertical velocity to represent settling ($\breve{w}$). Three size classes were implemented, a weightless tracer $C_{neutral}$ ($\breve{w}_{neutral}=0\,\mathrm{ms}^{-1}$), a clay fraction C_{clay} ($\breve{w}_{clay}=1.72\cdot10^{-6}\,\mathrm{ms}^{-1}$), and a silt fraction C_{silt} ($\breve{w}_{silt}=1.23\cdot10^{-4}\,\mathrm{ms}^{-1}$). Originally we also included a sand fraction ($\breve{w}_{sand}=3.47\cdot10^{-2}\,\mathrm{ms}^{-1}$), but this tracer settled out immediately below the source, and was found to lead to numerical instability. The weightless tracer is not being considered in this analysis. Aggregation processes like flocculation [*Feely*, 1976] that affect the transport of sediments are not taken into account. Sediment was introduced in the domain through a surface flux in La Plata estuary, with the same spatial pattern as the associated freshwater flux (indicated in Figure 3). The amplitude of the flux is set to an arbitrary value of $1\,\mathrm{gm}^{-2}\mathrm{s}^{-1}$.

The sedimentation rate S (bottom flux of sediment) is simply given by:

$$S=-\breve{w}\,C_b \tag{1}$$

where C_b is the concentration of a particular sediment class in the bottom layer. In an additional experiment, the sedimentation rate was reduced by a resuspension term, which is assumed proportional to the bottom stress. Classically, this would lead to a sedimentation rate of the form [*McCave and Swift*, 1976]:

$$S=-\breve{w}\,C_b\left(1-\frac{\tau}{\tau_c}\right) \tag{2}$$

where τ_c is a critical bottom stress, dependent on grain size, and $\tau=\rho_0 C_d|\mathbf{u_b}|\mathbf{u_b}$ is the actual bottom stress, with density scale $\rho_0(1\cdot10^3\,\mathrm{kgm}^{-3})$ and bottom velocity $\mathbf{u_b}$. However, this parameterization was found to be numerically unstable in areas where the model predicts net resuspension ($\tau>\tau_c$), so instead we implemented a monotonic variant of this parameterization as follows:

$$S=-\breve{w}\,C_b\Big/\left(1+\frac{\tau}{\tau_c}\right) \tag{3}$$

This formulation still allows for reduced sedimentation in energetic regions, but does not allow for net resuspension when $\tau>\tau_c$. For the bottom velocity $\mathbf{u_b}$, we average the velocity over the deepest 250 m, in order to reduce the impact of partial bottom cells and the imprint of the bathymetry on the results.

Initially, we applied a biharmonic diffusion operator to these tracers, but it was found to lead to nonmonotonic behavior; so instead we chose to apply a flux-limited advection scheme for horizontal transport. Vertical mixing is accomplished by the KPP scheme [*Large et al.*, 1994], which includes a depth-dependent

Figure 4. Divergence (black; mSv/m) of the horizontal volume flux across the boundary of the Zapiola Anticyclone (defined here as the $\Psi=0$ contour of the time-mean barotropic stream function in Figure 3). Gray contour shows area-integrated vertical transport (Sv).

background vertical diffusivity. In particular, vertical diffusivity κ_v increases from $0.25 \cdot 10^{-4}$ m^2s^{-1} at the surface to 0.85 $\cdot 10^{-4} m^2 s^{-1}$ at depth.

3. Results

3.1. Dynamics of the Zapiola Anticyclone

First we study the representation of the ZA in the model. Figure 3 shows the barotropic stream function (Ψ) in the AB. The circulation features a significant ZA centered around the ZR. The value $\Psi=0$ (indicated in red) represents about the lowest isoline that completely surrounds the ZR, and is considered here and in the remainder of this paper to be the boundary of the ZA. With this definition, the ZA represents a transport of no less than 272 Sv (but highly variable, with a standard deviation of 47 Sv). If we take the zero crossings of cumulative meridional transport at 50°W and 34°W in Figure 15 of *Saunders and King* [1995] as the boundaries of the observed ZA, then its strength appears to be 175 Sv. So the modeled ZA is 55% stronger than what seems to be the only direct observational estimate. The reason for this discrepancy is not clear, but it seems likely that an increase of the bottom drag would reduce the modeled ZA to a more realistic strength.

To study whether the secondary circulation associated with the ZA is consistent with theoretical considerations, we calculate the divergence of the horizontal velocity field at each depth, and integrate it over the ZA area. Figure 4 (black line) shows that the flow is convergent throughout the water column, except between 5 and 6 km depth, where the flow field is divergent (note that in this plot the bottom Ekman layer transport is smeared out vertically, as the depth along the rim of our ZA region varies between 5 and 6 km). This is consistent with the picture of *Dewar* [1998], where eddies cause a flow convergence over the seamount in their attempt to homogenize the potential vorticity field, which is balanced by a flow divergence in the bottom Ekman layer. The net vertical transport in the ZA increases with depth (gray) to push 4 Sv into the bottom layer.

The robustness of this behavior can be checked by calculating this flow convergence at a given depth for a series of increasing stream function values (and hence increasingly smaller areas around the ZA center). Figure 5 shows that the flow divergence at 3000 m is negative for each stream function contour, and so is the net vertical transport.

So despite the fact that the ZA simulated by the model is more than 50% stronger than observed, we believe that its dynamics are consistent with theoretical predictions. We therefore conclude that this model is adequate to study eddy-driven sediment dispersal in the AB.

3.2. Sediment Distribution

Figures 6 and 7 show the vertical distribution of the sediment concentration fields in austral summer (top) and winter (bottom) of year 6. There is a clear distinction between the distributions of the silt and clay fractions. In particular, the distribution of the silt fraction is quite homogeneous in the vertical, with concentrations highest at the bottom and lowest at the surface (Figure 6). The high settling rate $\breve{w}_{silt}=1.23 \cdot 10^{-4} ms^{-1}$ takes a silt grain to the bottom in about a year. The silt profile within the ZA (Figure 8a) shows that the supply of sediment to the ZA is very episodic.

The distribution of the clay fraction is in sharp contrast with that of the silt. The clay fraction is vertically stratified, and closely tied to the isopycnals. Even after 6 years, concentrations in the abyss are more than 8
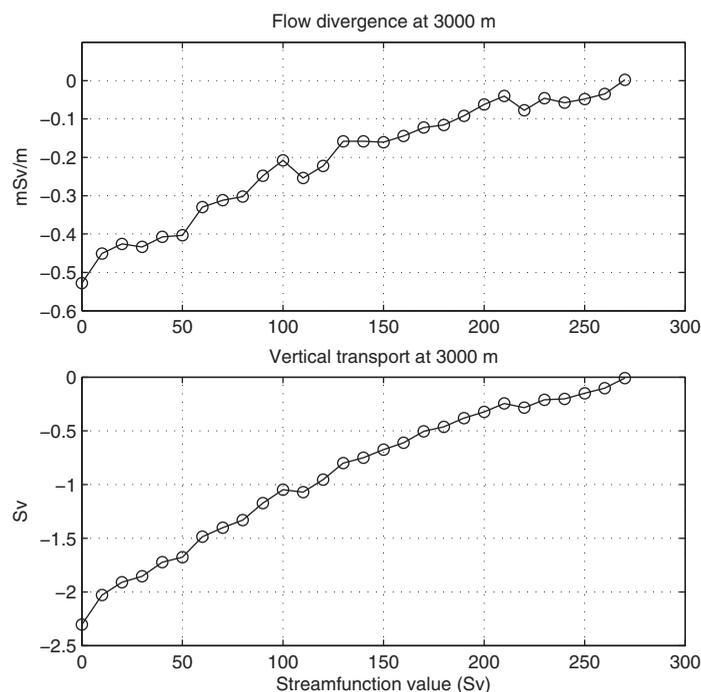
Figure 5. Divergence (top) of the horizontal volume flux at 3000 m depth, across a range of barotropic stream function contours. Vertical transport is shown in Figure 5 (bottom).

orders of magnitude smaller than at the surface. With the small settling velocity of $\breve{w}_{clay} = 1.72 \cdot 10^{-6} \text{ms}^{-1}$, it would take a clay particle 100 year to reach the bottom. This very slow penetration is also evident from the sediment concentration profile within the ZA (Figure 8b).

For both size fractions, full horizontal dispersion through the AB has been accomplished in just a few years. But despite this rapid horizontal dispersion, significant horizontal inhomogeneities exist. In particular, the sediment concentrations display a clear and persistent minimum over the ZR. The sequence of snapshots in Figure 9 gives a good impression of the dynamic nature of the sediment concentration fields, as it shows how a filament of sediment rich waters wraps around, and becomes entrained in the sediment starved center of the anticyclone.

The concentration minimum is persistent, as the sediment concentration within the ZA is consistently lower than on its perimeter almost everywhere and at any given time (Figure 8, hatching). An exception is the clay concentration in the upper 500 m, where interior concentrations exceed those on the rim episodically. Nonetheless, as explained in the Discussion section, full horizontal homogenization might not have been achieved within 6 years if horizontal diffusivities over the ZR are significantly reduced.
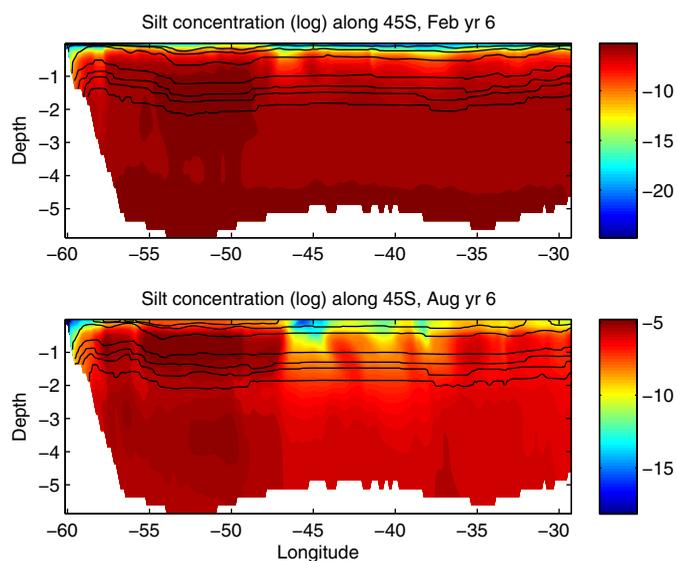
Figure 6. Distribution of the silt fraction ($\log(C_{silt})$), along 45°S across the Zapiola Rise. Monthly averages for February (top) and August (bottom) of year 6 of the simulation. Contours are select isopycnals.

3.3. Fluxes and Budgets

To study whether the volume convergence that drives the ZA plays a significant role in the sediment budget of ZR, we reconstruct the advective transport of sediment across the boundary of the ZA from the 5 daily snapshots of sediment concentration and velocity fields. In reconstructing the advective terms, we ignore the upwind character of the advective operator in the original code. In addition, by using 5 daily snapshots, we neglect covariances at higher frequencies. We found that this leads to normalized root mean square errors between 10 and 20% compared to the full fluxes
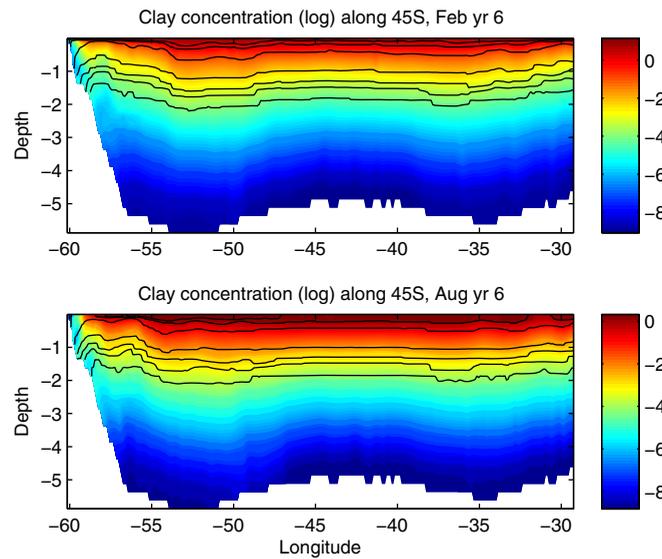
Figure 7. Distribution of the clay fraction ($\log(C_{clay})$) along 45°S across the Zapiola Rise. Monthly averages for February (top) and August (bottom) of year 6 of the simulation. Contours are select isopycnals.

(which were saved in monthly averages for years 5 and 6 only); still, the characteristics of the flux profiles presented here were found to be robust.

We use the divergence theorem to estimate the boundary integral of the sediment flux:

$$\oint \mathbf{u}C \cdot \mathbf{n}\, d\Gamma = \int \nabla \cdot \mathbf{u}C\, dA \quad (4)$$

where Γ is the contour defining the boundary of the ZA (the zero-contour of the barotropic stream-function), A is the area that it encloses, and $\mathbf{n}$ is the normal pointing outward. We separate the velocity field $\mathbf{u}$ into a time mean and an eddy component, $\mathbf{u} = \bar{\mathbf{u}} + \mathbf{u}'$, to give us two flux components:

$$\int \nabla \cdot \mathbf{u}C\, dA = \int \nabla \cdot \bar{\mathbf{u}}C\, dA + \int \nabla \cdot \mathbf{u}'C\, dA \quad (5)$$

If the ZA would be perfectly barotropic, $\bar{\mathbf{u}}$ would be perpendicular to $\mathbf{n}$ at all depths, and the contribution of the mean flow would be zero.

Another illustrative decomposition is:

$$\int \nabla \cdot \bar{\mathbf{u}}C\, dA = \int \bar{\mathbf{u}} \cdot \nabla C\, dA + \int C\nabla \cdot \bar{\mathbf{u}}\, dA \quad (6)$$

where the second term on the right-hand side reflects the effect of the net volume convergence that drives the ZA. Since the flux time series based on our 5 daily snapshots are very noisy, we focus on the *cumulative* flux since the start of the experiment.

Figure 10 shows the cumulative sediment flux divergence out of the ZA, for the silt (left) and clay (right) fractions, at 1875 and 3875 m depth. For the silt fraction, all flux divergences are negative throughout, indicating that the horizontal mean and eddy flow components transport silt into the ZA. The eddy component (red) dominates at both levels. The net volume flux convergence that drives the ZA generates a sediment convergence (green), as expected, but its contribution is small.

For the clay fraction, the situation is more complicated. At 1875 m the eddy contribution dominates, but at the deeper level, the

Figure 8. Distribution of the (a) silt (C_{silt}) and (b) clay ($\log(C_{clay})$) fractions, averaged over the ZA area. Shading indicates where $\Delta C = C_{perim} - C_{area} < 0$, hence where the sediment concentration within the ZA exceeds the concentration on the rim.
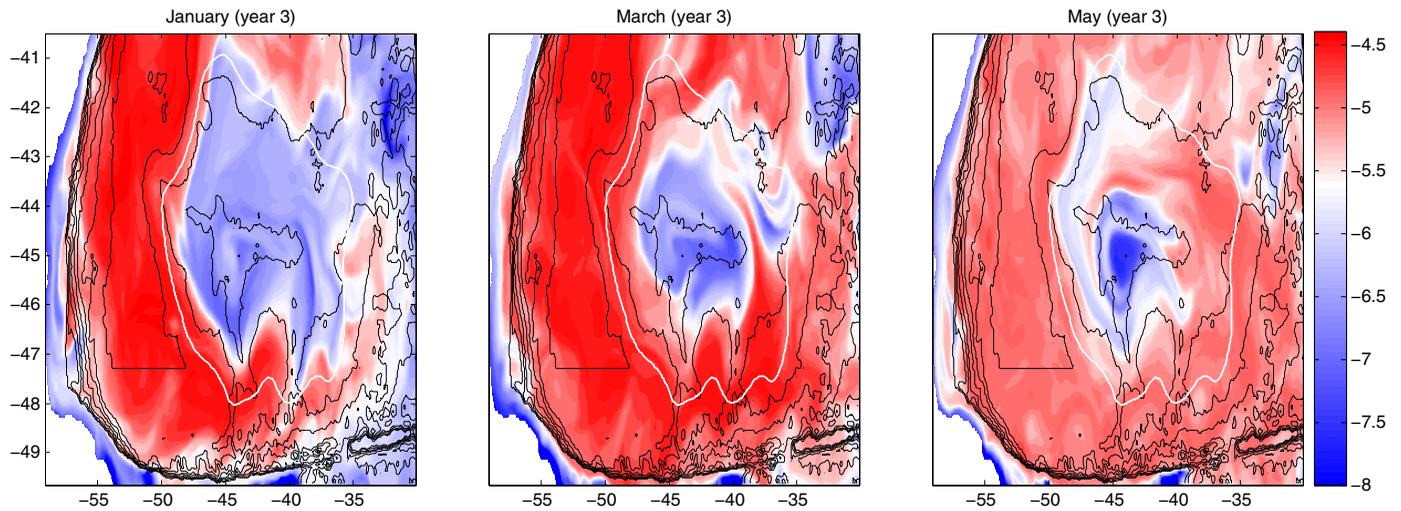
Figure 9. Distribution of the silt fraction ($\log(C_{silt})$) at 1600 m depth in year 3, for the months indicated. Black contours denote f/H, white contour shows the boundary of the Zapiola Anticyclone (defined as the zero contour of the time-mean barotropic stream function).
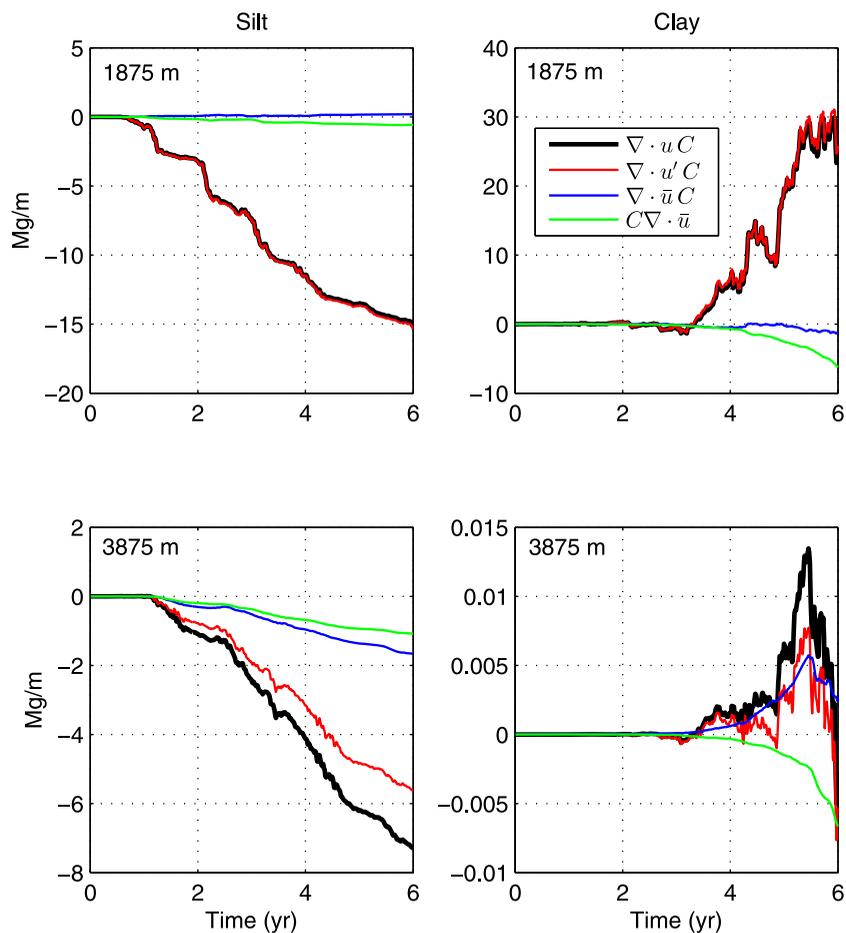
Figure 10. Cumulative divergence ($\mathrm{Mg\,m^{-1}}$) of the advective fluxes of silt (left) and clay (right), at 1875 m and 3875 m depth. Integration area A is the area enclosed by the $\Psi = 0$ contour of the barotropic stream function. Advective fluxes by the full velocity field (black) are separated in eddy (red) and mean (blue) contributions. In addition, the flux convergence is shown that results from the volume convergence that drives the ZA (green).
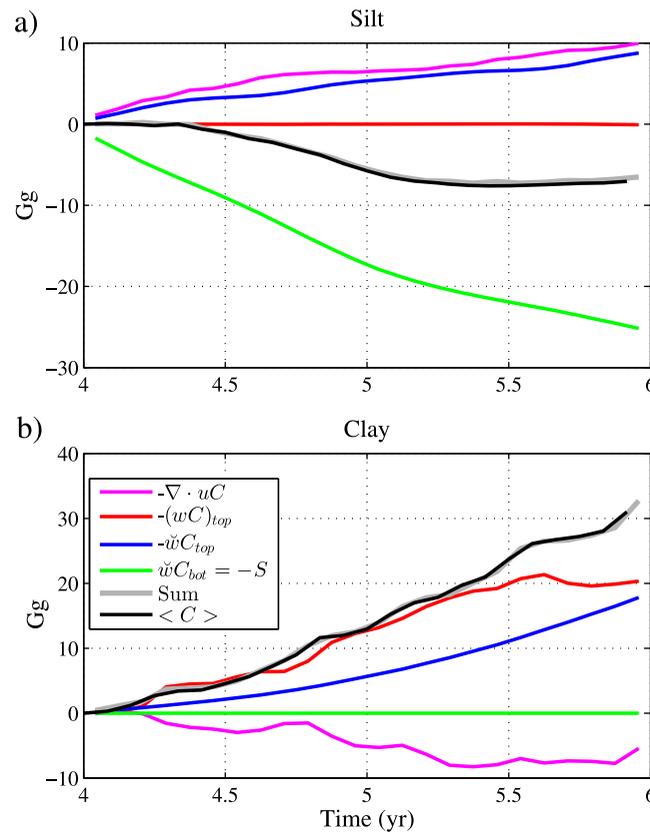
Figure 11. Sediment budget terms for the ZA column between 1875 and the bottom, for years 5 and 6. Curves show (black) the total sediment content (black; Gg); cumulative divergence of the horizontal advective fluxes (magenta); vertical advection through the top (red); settling flux through the top (blue) and bottom (green); and the sum of the flux components (gray). Advective fluxes through the bottom are zero.

contribution by the mean flow is of the same magnitude as the eddy component. What is more, the net sediment flux is *divergent*, hence transporting sediment out of the ZA. This is despite the fact that overall the sediment concentration is lower within the ZA than in its surroundings, so the eddy flux appears to be upgradient. This tendency seems to level off in year 5 at 1875 m, and to turn around at 3875 m. A longer integration would be required to check whether the advective clay flux eventually becomes convergent and downgradient.

To verify the robustness of the flux results, we calculated the overall terms in the sediment budget of the deep part of the ZA column, from 1875 to the bottom, and for years 5 and 6 (Figure 11). Only for these years were the horizontal fluxes saved as monthly averages, so they are more accurate than the reconstructions based on 5 daily means as shown in Figure 10. The fluxes are integrated from the start of year 5, so that their sum (gray) matches the evolution of sediment inventory (black) in the column:

$$\frac{d}{dt}\int C\,dV = -\int \nabla\cdot\mathbf{u}C\,dz - \int_{top} wC\,dA - \breve{w}\int_{top} C\,dA + \breve{w}\int_{bottom} C\,dA \qquad (7)$$

For the silt fraction (Figure 11a), settling through the bottom (sedimentation; green) is the dominant loss term for this part of the column, with horizontal convergence (magenta) and settling through the top (at 1875 m; blue) being the dominant source terms. Vertical advection through the top is negligible.

The situation for the clay fraction is in sharp contrast to that for silt (Figure 11b). Here, horizontal transport represents an actual loss term, confirming our conclusion based on Figure 10 (black lines, left column). This is counteracted by clay import due to settling and downward advection at the top of the column, significantly increasing the inventory of clay in the column. While the silt distribution has reached a quasisteady state, the clay fraction is far from equilibrated.

3.4. Discussion

The interaction between the turbulent flow in the Argentine Basin and the ZR is a fascinating problem. The control of the ZR on the circulation is well understood, as the ZA is a result of the tendency of eddies to undo the perturbation in the potential vorticity field induced by the seamount [*Dewar*, 1998]. However, it is not clear whether the circulation feeds back on the height of the ZR through its impact on sediment transport.

In this study, we set out to investigate the impact of the highly turbulent circulation in the AB on the sediment dispersal, with a specific focus on the ZA and the ZR. The numerical experiment shows that the ZA is

Figure 12. Sedimentation rates for silt (left; Mgm^{-2}s^{-1}) and clay (right; log-scale) in the ZR region. Shown are averages over years 5 and 6 of the standard simulation (top), and the branch simulation with modified sedimentation formulation (middle). Figure 12 (bottom) show the fractional difference between these fields, with $\Delta S = S^* - S$.

a barrier for the transport of sediments, and that the sediment concentrations within the ZA are persistently lower than in its surroundings. With a sedimentation parameterization that is simply proportional to the bottom sediment concentration (Eq. (1)), this results in *reduced* sediment deposition over the ZR compared to its immediate surroundings (Figure 12, top row).

The issue of horizontal (or rather, isopycnal) mixing by eddies is complex but important. Generic estimates of isopycnal diffusivity of the order of 10^3 m^{2}s^{-1} [e.g., *Marshall et al.*, 2006] may be significantly reduced in areas of strong mean flow [e.g., *Naveira Garabato et al.*, 2011]. *Bigorre* [2005] showed that, within the context of a quasigeostrophic model, these values may be one or two orders of magnitudes less within the ZA, dependent on the subgrid-scale mixing parameterization used. *Griesel et al.* [2010, 2014] analyzed diffusivities in the Subantarctic zone in the same model as used here (0.1° POP) but the spatial resolution of their results is too low to distinguish low values of diffusivity within the ZA from high values in the strongly eddying Brazil-Malvinas Confluence. Nevertheless, it is clear that eddy activity is significantly reduced over ZR (Figure 2).

If indeed diffusivities are significantly reduced over ZR, say, to values $\mathcal{O}(200$m^{2}s$^{-1})$ (as diagnosed by *Bigorre* [2005] for an eddy-resolving simulation with biharmonic closure), then a characteristic timescale of *horizontal* sediment dispersal may be $\mathcal{O}(25$yr), if we assume a length scale of $r = 5°$, or 400 km. That means that

a)

b)
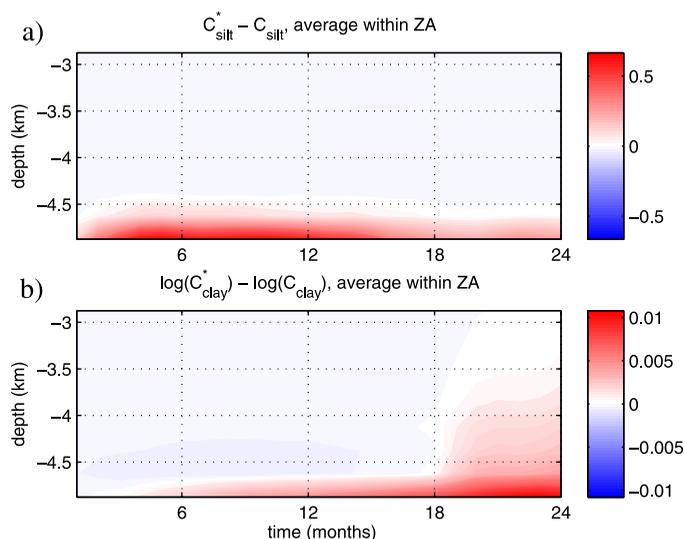
Figure 13. Concentrations of (a) silt and (b) clay (log) averaged over the ZA region, in the lower 1.5 km. Shown is the difference between the branch simulation with modified sedimentation parameterization, and the standard run.

even a 6 year integration may not have been enough to homogenize the silt field, if that were the only process in play. Yet, even if the sediment concentrations would be perfectly well-mixed within the AB, our simple sedimentation parameterization (equation (1)) would still not predict *preferred* sedimentation over the ZR. We therefore conclude that sediment transport by the turbulent interior ocean circulation alone is not able to explain enhanced deposition over the ZR.

The most obvious deficiency of the current model is that it lacks a detailed representation of the benthic boundary layer and sediment dynamics. In particular, bottom shear stresses can lead to resuspension, reducing the net sedimentation rate. The Argentine Basin is particularly well known for its deep nepheloid layer of suspended sediments that seems to be related to the high levels of eddy kinetic energy in the basin [*Richardson et al.*, 1993]. The impact of resuspension on net sedimentation can be expressed in the simplest form as equation (2) [*McCave and Swift*, 1976]. Indeed, eddy variability has a minimum over the ZR (Figure 2), which would be conducive to net sedimentation.

To make a first stab at studying the effect of resuspension, we repeated the final 2 years of the simulation (years 5 and 6) with an alternative formulation of the bottom sediment flux *S*, given by equation (3), with critical bottom stress $\tau_c = 0.05 \text{Nm}^{-2}$. We will indicate silt and clay concentrations of this branch run by C^*_{silt} and C^*_{clay}, respectively, and the respective sedimentation rates by S^*_{silt} and S^*_{clay}. Analysis of the results shows that the silt distribution adjusts quickly to the change in sedimentation parameterization, suggesting that we can draw firm conclusions based on these results. In contrast, the clay distribution is far from steady, and we can only get a tentative idea of the changes that would ensue if we were able to run the model long enough for the clay field to reach equilibrium.

Figures 12 and 13 show how the sedimentation parameterization affects sedimentation rates and sediment profiles. For the silt fraction, the largest anomalies in bottom concentration are recorded in the first year, apparently responding to interannual variability in sediment supplied to the ZA (Figure 13a). This suggests that the transient response to the change in sedimentation parameterization is accomplished within the first few months. This is confirmed by the difference in sedimentation pattern (Figure 12; left column): regions of reduced sedimentation alternate with regions of enhanced sedimentation. This pattern reflects a local reorganization of the sediment budget, as the *net* deposition over ZR is hardly affected (not shown). More importantly, even with the alternative sedimentation parameterization, sedimentation rates retain a clear minimum over ZR (Figure 12, middle).

This behavior is consistent with a simple scale analysis. If we assume that the model's nepheloid layer is governed mainly by vertical mixing and settling, then its thickness scales with $\delta = \kappa_v / \breve{w}$, and we can expect a thickness of just 0.7 m for silt (given the abyssal value $\kappa_v = 0.85 \cdot 10^{-4} \text{m}^2\text{s}^{-1}$ used in this model; for a high value of diffusivity of $\kappa_v = 1 \cdot 10^{-3} \text{m}^2\text{s}^{-1}$, this depth scale would still only be 8 m). An estimate of the time scale on which the layer would adjust is similarly given by $\tau = \kappa / \breve{w}^2$, which is about 2 h for silt. Given such a short adjustment time and small depth scale, it is unlikely that details of the sedimentation process could lead to the significant and large scale changes in the regional distribution of sediment that are necessary for ZR to become a *preferred* area for sedimentation.

The situation is different for clay. Deposition rates of clay decrease almost uniformly in the ZR region (Figure 12; right column). This causes a persistent increase of the clay concentration in the bottom layer, showing

Figure 14. Schematic representation of the simple model described in the text.

that it is far from equilibrium (Figure 13b). The expected nepheloid layer thickness, based on the above scale analysis, would be 50 m in the model, with an adjustment time of about a year. Such a layer thickness would clearly exceed a bottom Ekman layer depth, and make the sediment available for lateral transport. Indeed, an interesting aspect of Figure 13b is that after 18 months concentration anomalies appear higher up in the water column. These anomalies are due to horizontal (isopycnal) advection, rather than the local, one-dimensional balance as discussed above. This is of course consistent with observed nepheloid layer thickness in the AB, which is of order $\mathcal{O}(1\text{km})$ [*Ewing et al.*, 1971; *McCave*, 1986; *Richardson et al.*, 1993].

Equation (2) tells us that ZR could be a *preferred* location for sedimentation if the bottom shear stresses induced by eddy activity are low enough to compensate for the reduced concentrations inside the ZA. This trade-off between a low enough concentration in the ZA core to sustain a significant eddy-driven influx, and a high enough concentration to generate a sizeable sedimentation rate can be illustrated by a very simple model (Figure 14). Consider the ZA as a cylinder with radius r and height H, with homogenous sediment concentration c that settles out at rate $S = \breve{w}\,c$. The sediment outside the column is of concentration c_0 and rains out at a rate $S_0 = \breve{w}_0 c_0$. A lateral exchange between the column and its surroundings is given by $F = \kappa(c_0 - c)/r$, with eddy diffusivity κ. In steady state, the lateral flux into the column is balanced by sedimentation, according to:

$$2\kappa H(c_0 - c) - \breve{w}\,cr^2 = 0 \tag{8}$$

where the appropriate metric terms are taken into account. We assume that sediment concentration within the column is lower than its surroundings, so $c = \alpha c_0$ with $\alpha < 1$. We also assume that the settling rate outside the ZA is lower than inside, so that $\breve{w}_0 = \beta\breve{w}$, where $\beta < 1$ is an attenuation factor due to resuspension in the more energetic surrounding environment. The condition of preferred sedimentation within ZA can now be expressed as:

$$\frac{\breve{w}\,c}{\breve{w}_0 c_0} = \frac{\alpha}{\beta} > 1 \tag{9}$$

which translates to:

$$\beta < \frac{1}{1+\gamma} \quad \text{with} \quad \gamma = \frac{\breve{w}\,r^2}{2\kappa H} \tag{10}$$

Filling in some generic values, $\kappa = 2 \cdot 10^2\,\text{m}^2\text{s}^{-1}$, $H = 5000\,\text{m}$, $r_0 = 4 \cdot 10^5\,\text{m}$, and $\breve{w} = \breve{w}_{clay} = 1.72 \cdot 10^{-6}\,\text{ms}^{-1}$, we arrive at $\beta < 0.88$. So if in this example sedimentation outside the ZA is suppressed by a very reasonable 12%, then the ZR can be a region of preferred sedimentation. Whether ultimately the condition can be met for clay can only be tested by much longer simulations that allow for appropriate equilibration of the clay distribution.

There are other processes missing from the current model that may be relevant for the growth of the ZR. Sediment convergence over ZR could be related to the intense mud wave activity in the region. Both observational and modeling studies suggest that these mud waves propagate upslope and upcurrent [*Flood and Shor*, 1988; *Flood*, 1988; *Blumsack and Weatherly*, 1989; *von Lom-Keil et al.*, 2002]. However, the direction of mud wave propagation does not necessarily reflect the direction of sediment transport, and a net bed load transport that is both upcurrent and upslope seems energetically unsustainable [*Bailard*, 1981].

Yet, studies of the circulation in shallow, tide-dominated seas have shown that nonlinear rectification can lead to a residual circulation that is upslope with respect to bathymetric features [*Zimmerman*, 1981; *Maas*

and Zimmerman, 1989; *Chen and Beardsley*, 1995]. It is possible that a similar nonlinear rectification of the eddy circulation around the ZR generates upslope transport, opposing the Ekman flow. In the current model, such a rectified circulation, if present, is not strong enough to counteract the strong Ekman transport in the bottom layer (Figure 4). A more detailed comparison with tidal rectification models might illustrate whether this mechanism carries over from tides to eddies, and from shallow seas with relatively small bathymetric disturbances to deep ocean basins with $\mathcal{O}(1\mathrm{km})$ bathymetric features.

The tight coupling between ocean circulation, sediment transport, and bathymetry raises the question how this coupled system originated. It seems likely that, ever since the installment of the modern ocean circulation, the BMC has persistently provided high levels of eddy kinetic energy to the Argentine Basin, hence providing an effective means of suspended sediment transport into the interior of the Argentine Basin. It is similarly likely that AABW has been flowing north in a western boundary current along the continental margin. So bottom kinetic energy (of the mean flow) must have exhibited a maximum close to the continent, decreasing toward more quiescent conditions farther offshore. So it is possible that the inflow of AABW alone could have facilitated enhanced sedimentation offshore from its western boundary current, initiating a proto-Zapiola Rise that subsequently grew into the prominent bathymetric feature that it is today.

4. Conclusions

In this paper, we tested the hypothesis that the transport of sediments by the highly turbulent circulation in the Argentine Basin is responsible for the enhanced accumulation of sediments over the Zapiola Rise, and hence is a key factor in the existence, and possibly continued growth of this seamount. However, in our model the Zapiola Anticyclone, a vortex that is trapped around the Zapiola Rise, is a barrier to sediment transport. Preferred sedimentation can therefore not be explained by eddy-driven transports alone. Details of sedimentation dynamics are probably essential to explain the existence and growth of the ZR.

References

Adcroft, A., C. Hill, and J. Marshall (1997), Representation of topography by shaved cells in a height coordinate ocean model, *Mon. Weather Rev.*, *125*(9), 2293–2315.

Allen, G. P., J. Salomon, P. Bassoullet, Y. Du Penhoat, and C. De Grandpre (1980), Effects of tides on mixing and suspended sediment transport in macrotidal estuaries, *Sediment. Geol.*, *26*(1), 69–90.

Bailard, J. A. (1981), An energetics total load sediment transport model for a plane sloping beach, *J. Geophys. Res.*, *86*(C11), 10,938–10,954.

Balsam, W. L., and R. J. Wolhart (1993), Sediment dispersal in the Argentine Basin: Evidence from visible light spectra, *Deep Sea Res., Part II*, *40*, 1001–1031.

Barnier, B., et al. (2006), Impact of partial steps and momentum advection schemes in a global ocean circulation model at eddy permitting resolution, *Ocean Dyn.*, *56*, 543–567.

Bigorre, S. (2005), Topographic effects on wind driven ocean circulation, PhD thesis, Florida State Univ., Tallahassee, Fla.

Bigorre, S., and W. K. Dewar (2009), Oceanic time variability near a large scale topographic circulation, *Ocean Modell.*, *29*, 176–188.

Biscaye, P. E. (1965), Mineralogy and sedimentation of recent deep-sea clay in the Atlantic Ocean and adjacent seas and oceans, *Geol. Soc. Am. Bull.*, *76*, 803–832.

Biscaye, P. E., and S. L. Eittreim (1977), Suspended particulate loads and transports in the nepheloid layer of the abyssal Atlantic Ocean, *Dev. Sedimentol.*, *23*, 155–172.

Blumsack, S. L., and G. L. Weatherly (1989), Observations of the nearby flow and a model for the growth of mudwaves, *Deep Sea Res., Part A*, *36*, 1327–1339.

Boebel, O., R. E. Davis, M. Ollitrault, R. G. Peterson, P. L. Richardson, C. Schmid, and W. Zenk (1999), The intermediate depth circulation of the western South Atlantic, *Geophys. Res. Lett.*, *26*(21), 3329–3332.

Chen, C., and R. C. Beardsley (1995), A numerical study of stratified tidal rectification over finite-amplitude banks. Part i: Symmetric banks, *J. Phys. Oceanogr.*, *25*(9), 2090–2110.

Combes, V., and R. P. Matano (2014), A two-way nested simulation of the oceanic circulation in the Southwestern Atlantic, *J. Geophys. Res. Oceans*, *119*, 731–756, doi:10.1002/2013JC009498.

De Miranda, A. P., B. Barnier, and W. K. Dewar (1999), On the dynamics of the Zapiola Anticyclone, *J. Geophys. Res.*, *104*(C9), 21,137–21,149.

Dewar, W. K. (1998), Topography and barotropic transport control by bottom friction, *J. Mar. Res.*, *56*, 295–328.

Dukowicz, J. K., and R. D. Smith (1994), Implicit free-surface method for the Bryan-Cox-Semtner ocean model, *J. Geophys. Res.*, *99*(C4), 7991–8014.

Ewing, M. (1965), The sediments of the Argentine Basin (Harold Jeffreys Lecture), *Q. J. R. Astron. Soc.*, *6*, 10–27.

Ewing, M., and A. G. Lonardi (1971), Sediment transport and distribution in the Argentine Basin. 5. Sedimentary structure of the Argentine margin, basin, and related provinces, *Phys. Chem. Earth*, *84*, 123–251.

Ewing, M., W. J. Ludwig, and J. I. Ewing (1964), Sediment distribution in the oceans: The Argentine Basin, *J. Geophys. Res.*, *69*(10), 2003–2032.

Ewing, M., S. L. Eittreim, J. I. Ewing, and X. Le Pichon (1971), Sediment transport and distribution in the Argentine Basin. 3. Nepheloid layer and processes of sedimentation, *Phys. Chem. Earth*, *84*, 51–77.

Feely, R. A. (1976), Evidence for aggregate formation in a nepheloid layer and its possible role in the sedimentation of particulate matter, *Mar. Geol.*, *20*(2), 7–13.

Fekete, B. M., C. J. Vörösmarty, and W. Grabs (1999), Global, composite runoff fields based on observed river and simulated water balances, technical report 22, Global Runoff Data Cent., Koblenz, Germany.

Flood, R. D. (1988), A lee wave model for deep-sea mudwave activity, *Deep Sea Res., Part A 35*, 973–983.

Flood, R. D., and A. N. Shor (1988), Mudwaves in the Argentine Basin and their relationship to regional bottom circulation patterns, *Deep Sea Res., Part A, 35*, 943–971.

Flood, R. D., A. N. Schor, and P. L. Manley (1993), Morphology of abyssal mudwaves at project MUDWAVES sites in the Argentine Basin, *Deep Sea Res., Part II, 40*, 859–888.

Fu, L.-L. (2006), Pathways of eddies in the South Atlantic Ocean revealed from satellite altimeter observations, *Geophys. Res. Lett., 33*, L14610, doi:10.1029/2006GL026245.

Fu, L.-L., and R. D. Smith (1996), Global ocean circulation from satellite altimetry and high-resolution computer simulation, *Bull. Am. Meteorol. Soc., 77*, 2625–2636.

Gaiero, D. M., J.-L. Probst, P. Depetris, S. Bidart, and L. Leleyter (2003), Iron and other transition metals in Patagonian riverborne and windborne materials: Geochemical control and transport to the southern South Atlantic Ocean, *Geochim. Cosmochim. Acta, 67*(19), 3603–3623.

Garzoli, S., and C. Giulivi (1994), What forces the variability of the southwestern Atlantic boundary currents?, *Deep Sea Res., Part I, 41*(10), 1527–1550.

Garzoli, S., and C. Simionato (1990), Baroclinic instabilities and forced oscillations in the Brazil/Malvinas confluence front, *Deep Sea Res., Part A, 37*, 1053–1074.

Garzoli, S. L. (1993), Geostrophic velocity and transport variability in the brazil-malvinas confluence, *Deep Sea Res., Part I, 40*, 1379–1403.

Glorioso, P. D., and R. A. Flather (1995), A barotropic model of the currents off SE South America, *J. Geophys. Res., 100*(C7), 13,427–13,440.

Glorioso, P. D., and R. A. Flather (1997), The Patagonian shelf tides, *Prog. Oceanogr., 40*(1), 263–283.

Griesel, A., S. T. Gille, J. Sprintall, J. L. McClean, J. H. LaCasce, and M. E. Maltrud (2010), Isopycnal diffusivities in the Antarctic Circumpolar Current inferred from Lagrangian floats in an eddying model, *J. Geophys. Res., 115*, C06006, doi:10.1029/2009JC005821.

Griesel, A., J. McClean, S. Gille, J. Sprintall, and C. Eden (2014), Eulerian and Lagrangian isopycnal eddy diffusivities in the Southern Ocean of an eddying model, *J. Phys. Oceanogr., 44*(2), 644–661.

Hurrell, J. W., J. J. Hack, D. Shea, J. M. Caron, and J. Rosinski (2008), A new sea surface temperature and sea ice boundary dataset for the community atmosphere model, *J. Clim., 21*(19), 5145–5153.

Jones, G. A., and D. A. Johnson (1984), Displaced Antarctic diatoms in Vema Channel sediments: Late Pleistocene/Holocene fluctuations in AABW flow, *Mar. Geol., 58*, 165–186.

Jullion, L., K. J. Heywood, A. C. Naveira Garabato, and D. P. Stevens (2010), Circulation and water mass modification in the Brazil-Malvinas Confluence, *J. Phys. Oceanogr., 40*, 845–864.

Klaus, A., and M. T. Ledbetter (1988), Deep-sea sedimentary processes in the Argentine Basin revealed by high-resolution seismic records (3.5 kHz echograms), *Deep Sea Res., Part A, 35*, 899–917.

Krinsley, D., P. E. Biscaye, and K. K. Turekian (1973), Argentine Basin sediment sources as indicated by quartz surface textures, *J. Sediment. Res., 43*(1), 251–257.

Large, W. G., and S. Pond (1982), Sensible and latent heat flux measurements over the ocean, *J. Phys. Oceanogr., 12*(5), 464–482.

Large, W. G., and S. Yeager (2004), Diurnal to decadal global forcing for ocean and sea-ice models: The data sets and flux climatologies, technical report NCAR/TN-460+STR, Natl. Cent. for Atmos. Res., Boulder, Colo.

Large, W. G., J. C. McWilliams, and S. C. Doney (1994), Oceanic vertical mixing: A review and a model with nonlocal boundary layer parameters, *Rev. Geophys., 32*(4), 363–403.

Le Pichon, X., S. Eittreim, and W. J. Ludwig (1971), Sediment transport and distribution in the Argentine Basin. 1. Antarctic bottom current passage through the Falkland fracture zone, *Phys. Chem. Earth, 84*, 1–28.

Ledbetter, M. T. (1986), Bottom-current pathways in the Argentine Basin revealed by mean silt particle size, *Nature, 321*, 423–425.

Lonardi, A. G., and M. Ewing (1971), Sediment transport and distribution in the Argentine Basin. 4. Bathymetry of the continental margin, Argentine Basin and other related provinces. Canyons and sources of sediments, *Phys. Chem. Earth, 84*, 79–121.

Maas, L., and J. Zimmerman (1989), Tide-topography interactions in a stratified shelf sea ii. Bottom trapped internal tides and baroclinic residual currents, *Geophys. Astrophys. Fluid Dyn., 45*(1–2), 37–69.

Mahowald, N. M., A. R. Baker, G. Bergametti, N. Brooks, R. a. Duce, T. D. Jickells, N. Kubilay, J. M. Prospero, and I. Tegen (2005), Atmospheric global dust cycle and iron inputs to the ocean, *Global Biogeochem. Cycles, 19*, GB4025, doi:10.1029/2004GB002402.

Maltrud, M., F. Bryan, and S. Peacock (2010), Boundary impulse response functions in a century-long eddying global ocean simulation, *Environ. Fluid Mech., 10*, 275–295.

Maltrud, M. E., F. Bryan, M. Hecht, E. Hunke, D. Ivanova, J. McClean, and S. Peacock (2008), Global ocean modelling in the eddying regime using POP, *CLIVAR Exch. Newsl., 44*, 5–8.

Manley, P. L., and R. D. Flood (1993), Paleoflow history determined from mudwave migration: Argentine Basin, *Deep Sea Res., Part II, 40*, 1033–1055.

Marshall, J., E. Shuckburgh, H. Jones, and C. Hill (2006), Estimates and implications of surface eddy diffusivity in the Southern Ocean derived from tracer transport, *J. Phys. Oceanogr., 36*, 1806–1821.

Matano, R., E. Palma, and A. Piola (2010), The influence of the Brazil and Malvinas Currents on the southwestern Atlantic shelf circulation, *Ocean Sci., 6*(4), 983–995.

Matano, R. P., et al. (2014), The salinity signature of the cross-shelf exchanges in the Southwestern Atlantic Ocean: Numerical simulations, *J. Geophys. Res. Oceans, 119*, 7949–7968, doi:10.1002/2014JC010116.

Maximenko, N., P. Niiler, L. Centurioni, M.-H. Rio, O. Melnichenko, D. Chambers, V. Zlotnicki, and B. Galperin (2009), Mean dynamic topography of the ocean derived from satellite and drifting buoy data using three different techniques, *J. Atmos. Oceanic Technol., 26*, 1910–1919.

Mazloff, M. R., P. Heimbach, and C. Wunsch (2010), An eddy-permitting Southern Ocean state estimate, *J. Phys. Oceanogr., 40*, 880–899.

McCave, I. N. (1986), Local and global aspects of the bottom nepheloid layers in the world ocean, *Neth. J. Sea Res., 20*, 167–181.

McCave, I. N., and S. A. Swift (1976), A physical model for the rate of deposition of fine-grained sediments in the deep sea, *Geol. Soc. Am. Bull., 87*, 541–546.

Milliman, J. D., and R. H. Meade (1983), World-wide delivery of river sediment to the oceans, *J. Geol., 91*, 1–21.

Naveira Garabato, A. C., R. Ferrari, and K. L. Polzin (2011), Eddy stirring in the Southern Ocean, *J. Geophys. Res., 116*, C09019, doi:10.1029/2010JC006818.

Palma, E. D., R. P. Matano, and A. R. Piola (2004), A numerical study of the Southwestern Atlantic Shelf circulation: Barotropic response to tidal and wind forcing, *J. Geophys. Res., 109*, C08014, doi:10.1029/2004JC002315.

Penduff, T., B. Barnier, K. Béranger, and J. Verron (2001), Comparison of near-surface mean and eddy flows from two numerical models of the South Atlantic Ocean, *J. Geophys. Res.*, *106*(C8), 16,857–16,867.

Penduff, T., P. Brasseur, C.-E. Testut, B. Barnier, and J. Verron (2002), A four-year eddy-permitting assimilation of sea-surface temperature and altimetric data in the South Atlantic Ocean, *J. Mar. Res.*, *60*, 805–833.

Penduff, T., J. Le Sommer, B. Barnier, A.-M. Treguier, J.-M. Molines, and G. Madec (2007), Influence of numerical schemes on current-topography interactions in 1/4° global ocean simulations, *Ocean Sci.*, *3*, 509–524.

Peterson, R. G. (1992), The boundary currents in the western Argentine Basin, *Deep Sea Res., Part A*, *39*, 623–644.

Peterson, R. G., and L. Stramma (1991), Upper-level circulation in the South Atlantic Ocean, *Prog. Oceanogr.*, *26*, 1–73.

Pierce, J., and F. R. Siegel (1979), Supended particulate matter on the southern argentine shelf, *Mar. Geol.*, *29*(1), 73–91.

Piola, A. R., R. P. Matano, E. D. Palma, O. O. Möller, and E. J. Campos (2005), The influence of the Plata River discharge on the western South Atlantic shelf, *Geophys. Res. Lett.*, *32*, L01603, doi:10.1029/2004GL021638.

Reid, J. L. (1989), On the total geostrophic circulation of the South Atlantic Ocean: Flow patterns, tracers and transports, *Prog. Oceanogr.*, *23*, 149–244.

Richardson, M. J., G. L. Weatherly, and W. D. Gardner (1993), Benthic storms in the Argentine Basin, *Deep Sea Res., Part II*, *40*, 975–987.

Romero, O., and C. Hensen (2002), Oceanographic control of biogenic opal and diatoms in surface sediments of the Southwestern Atlantic, *Mar. Geol.*, *186*, 263–280.

Saraceno, M., C. Provost, and U. Zajaczkovski (2009), Long-term variation in the anticyclonic ocean circulation over the Zapiola Rise as observed by satellite altimetry: Evidence of possible collapses, *Deep Sea Res., Part I*, *56*, 1077–1092.

Saunders, P. M., and B. A. King (1995), Bottom currents derived from shipborne ADCP on WOCE cruise A11 in the South Atlantic, *J. Phys. Oceanogr.*, *25*, 329–347.

Venaille, A., J. Le Sommer, J.-M. Molines, and B. Barnier (2011), Stochastic variability of oceanic flows above topography anomalies, *Geophys. Res. Lett.*, *38*, L16611, doi:10.1029/2011GL048401.

Volkov, D. L., and L.-L. Fu (2008), The role of vorticity fluxes in the dynamics of the Zapiola Anticyclone, *J. Geophys. Res.*, *113*, C11015, doi:10.1029/2008JC004841.

von Lom-Keil, H., V. Spieß, and V. Hopfauf (2002), Fine-grained sediment waves on the western flank of the Zapiola Drift, Argentine Basin: Evidence for variations in Late Quaternary bottom flow activity, *Mar. Geol.*, *192*, 239–258.

Weatherly, G. L. (1984), An estimate of bottom frictional dissipation by Gulf Stream fluctuations, *J. Mar. Res.*, *42*(2), 289–301.

Weatherly, G. L. (1993), On deep-current and hydrographic observations from a mudwave region and elsewhere in the Argentine Basin, *Deep Sea Res., Part II*, *40*, 939–961.

Weijer, W., M. E. Maltrud, M. W. Hecht, H. A. Dijkstra, and M. A. Kliphuis (2012), Response of the Atlantic Ocean circulation to Greenland Ice Sheet melting in a strongly-eddying ocean model, *Geophys. Res. Lett.*, *39*, L09606, doi:10.1029/2012GL051611.

Whittaker, J., A. Goncharov, S. Williams, R. D. Müller, and G. Leitchenkov (2013), Global sediment thickness dataset updated for the Australian-Antarctic Southern Ocean, *Geochem. Geophys. Geosyst.*, *14*, 3297–3305, doi:10.1002/ggge.20181.

Zimmerman, H. B., P. R. Supko, and F. W. McCoy (1979), Acoustic horizons in the Argentine Basin, southwestern Atlantic Ocean: New evidence from deep-sea drilling, *Geology*, *7*, 45–48.

Zimmerman, J. (1981), Dynamics, diffusion and geomorphological significance of tidal residual eddies, *Nature*, *290*, 549–555.